Electrochemical Behavior of Plasma Nitrided Austenitic Stainless Steel in Chloride Solutions

Viera Zatkalíková *, Petra Drímalová, Katarzyna Balin, Martin Slezák, Lenka Markovičová

Posted Date: 12 July 2024

doi: 10.20944/preprints202407.0971.v1

Keywords: austenitic stainless steel; plasma nitriding; corrosion resistance; potentiodynamic polarization; electrochemical impedance spectroscopy

Article

Electrochemical Behavior of Plasma Nitrided Austenitic Stainless Steel in Chloride Solutions

Viera Zatkalíková [1,*], Petra Drímalová [1], Katarzyna Balin [2], Martin Slezák [1] and Lenka Markovičová [1]

[1] Department of Materials Engineering, Faculty of Mechanical Engineering, University of Žilina, Univerzitná 8215/1, 010 26 Žilina, Slovakia; martin.slezak@fstroj.uniza.sk (M.S.); petra.drimalova@fstroj.uniza.sk (P.D.); lenka.markovicova@fstroj.uniza.sk (L.M.)

[2] A. Chełkowski Institute of Physics University of Silesia in Katowice, 75 Pułku Piechoty 1, Chorzów, Poland; katarzyna.balin@us.edu.pl (K.B.)

* Correspondence: viera.zatkalikova@fstroj.uniza.sk; Tel.: +421-41-513-2610

Abstract: The application possibilities of austenitic stainless steels in high friction, abrasion and sliding wear conditions are limited by their inadequate hardness and tribological characteristics. In order to improve these properties, thermochemical treatment of their surface by plasma nitriding is suitable. This article is focused on corrosion resistance of the conventionally plasma nitrided AISI 304 stainless steel (530 °C, 24 hours) in 0.05 M and 0.5 M sodium chloride solutions at room temperature (20 ± 3 °C), tested by potentiodynamic polarization and electrochemical impedance spectroscopy. The optical microscopy, scanning electron microscopy, energy-dispersive X-ray spectroscopy and X-ray photoelectron spectroscopy are used for the nitrided layer characterization. The experiment results point to a significant reduction in corrosion resistance after performed plasma nitriding even in a solution with a very low chloride concentration (0.05 mol/L).

Keywords: austenitic stainless steel; plasma nitriding; corrosion resistance; potentiodynamic polarization; electrochemical impedance spectroscopy

1. Introduction

Austenitic stainless steels are commonly used in various fields of human activity because of the combination of high corrosion resistance and satisfactory mechanical properties. However, their utilization as a construction material in applications where subjected to friction, abrasion, or sliding wear is limited by their insufficient hardness and poor tribological properties [1–4]. The above problem can be solved by nitriding that involves the diffusion of nitrogen into the material surface layer. The nitrided surface has increased hardness and can exhibit lower friction coefficients, reducing friction between moving parts. This contributes to improved efficiency and reduced energy consumption. Additionally, the nitrided layer can act as a solid lubricant in some cases [5–7]. Older methods of nitriding were economically demanding and caused distinctive environmental problems [8–10].

Plasma nitriding (PN) takes place in ionized gases ($N_2 + H_2$, NH_3) at reduced pressure under the influence of an electric field. It is less time consuming and environmentally friendly because it typically uses fewer hazardous chemicals than previous nitriding methods and produces minimal waste [6,7,11–13]. By improving hardness and wear resistance, plasma nitriding helps extend the life of austenitic stainless steel components, which is critical in industries where durability and longevity are essential factors [11–15].

PN of stainless steels has been the subject of research for several decades and many specific methods based on it are currently in use. The choice of method depends on factors such as the material being treated, the desired outcome, and the characteristics of the components undergoing nitriding. The ways of PN differ especially in key process parameters (temperature, gas composition, pressure, and treatment duration), which affect the resulting properties of the nitrided stainless steel

 doi:10.20944/preprints202407.0971.v1

surfaces [14–18]. The obtained hardness is influenced mainly by the nitriding temperature used, and depends on precipitation of hard chromium nitrides, that are typically formed at the temperatures above 500 °C. Therefore, this conventional high-temperature plasma nitriding brings significant increase of hardness and a high resistance to wear, but due to depletion of chromium, corrosion resistance is limited [11,16–24]. After high-temperature PN the loss of passive behavior of austenitic SS in potentiodynamic polarization has been observed by several authors [6,13,15,16]. In some cases, high-temperature nitriding can also lead to a martensitic transformation of the austenitic structure [25,26]. Because martensite is a harder phase than austenite, further enhancing the material's hardness continues [27].

However, if the nitriding temperature is around 400 °C (so-called low-temperature nitriding) an expanded austenite ("S" phase) as an oversaturated solid solution of nitrogen in the austenitic face-centered cubic lattice is created [11–13,17,18,20,22,24]. This process is not accompanied by chromium depletion and material retains its high corrosion resistance [12,17–20]. A decrease of susceptibility to the pitting corrosion in chloride solutions after low-temperature nitriding was confirmed by authors [21–23]. The expanded austenite contributes to increased hardness, but the effect is not as significant as the formation of hard chromium nitrides [7,11,15]. Moreover a considerable amount of residual austenite may still leave in the structure. The authors [15] noted that the micro-hardness of AISI 316L stainless steel after 4-hours low-temperature nitriding at 400 °C (about 580 HV) is approximately half that observed in high-temperature nitriding at 520 °C (about 1200 HV). The choice between low and high-temperature austenitic stainless steels plasma nitriding depends on the specific application requirements. If, in addition to improved tribological properties maintaining the austenitic structure and low susceptibility to a corrosion are important, low-temperature nitriding may be preferred. For maximum hardness and wear resistance, high-temperature nitriding is more suitable. A compromise between low-temperature and high-temperature nitriding is rapid short-term high-temperature nitriding, which results in a nitrided layer that contains both expanded austenite and chromium nitrides [28,29].

The presented paper deals with properties of plasma nitrided AISI 304 stainless steel. The main aim is to assess to what extent the conventional plasma nitriding (530 °C, 24 hours) reduces the corrosion resistance of a given material in chloride solutions dependent on chloride concentration used. The plasma nitrided layer is characterized by optical microscope (OM), SEM, EDX and X-ray photoelectron spectroscopy (XPS). The evaluation of corrosion resistance is based on potentiodynamic polarization (PP) and electrochemical impedance spectroscopy (EIS) both carried out in 0.05 M and 0.5 M sodium chloride solution at room temperature (20 ± 3 °C).

2. Materials and Methods

The experimental material AISI 304 was purchased as a 1.5 mm thick sheet with a smooth and matt surface (2B surface finish) and the following chemical composition (wt.%) specified by atomic emission spectrometry (Spectromaxx analyzer): Cr 19.09, Ni 8.15, Mn 1.33, N 0.074, C 0.03, Si 0.37, P 0.029, S 0.004, Fe balance.

For PN process, the rectangular specimens with dimensions 15 mm x 40 mm x 1.5 mm were prepared. A part of the specimens was left in their original state ("as received state") for a comparison of the obtained tests results. The surfaces of the specimens to be nitrided were not mechanically or chemically treated, only rinsed with water and ethanol and then dried with a stream of air.

PN process was performed in the specialized laboratory of RUBIG SK, k. s. in a plasma nitriding furnace. The recipient (furnace casing) was connected to the circuit as an anode. The process lasted 24 hours and was carried out at a temperature of 530 °C. The process included argon dusting. The nitriding was followed by cooling to a temperature of 160 °C, after which the pressure was equilibrated to atmospheric pressure and nitrided specimens were cooled freely to a common laboratory temperature.

For characterization, the nitrided specimen surface was displayed and EDX mapping analysed by Tescan Vega scanning electron microscope (SEM). The cross-section of plasma nitrided specimen was observed by optical microscope (OM) after glycerine + HNO_3 + HF etching.

 doi:10.20944/preprints202407.0971.v1

The presence of chromium nitrides and the prevalent type were determined by XPS analysis performed in a specialized laboratory of A. Chełkowski Institute of Physics, University of Silesia (Katowice, Poland) using Physical Electronic XPS spectrometer (Physical Electronics PHI 5700). For photoelectron excitation the X-Ray $Al_{K\alpha 1}$ monochromatic radiation with energy of 1486 eV was used. The photoelectron survey and high-resolution spectra were collected form 80 μm in diameter areas before and after surface cleaning (Ar^+, 1.5 kV, 20 mA, 5 min). The photoelectron spectra were analyzed using MULTIPAK (v.9.6.0.1, ULVAC PHI) software. The high-resolution spectra were calibrated using the C1s peak (284.6 eV).

The Vickers microhardness evaluation of the plasma nitrided sample was performed using a Zwick/Roell ZHVμ microhardness tester with a load of 0.01 kp (HV0.01 = 0.0981 N) and with a 10-second action of the indenter. For better visibility of the resulting indentations, the specimen was metallographically prepared (withougth etching) before the microhardness measurement.

Corrosion tests were carried out at the temperature 20 ± 3 °C in pH neutral 0.05 M and 0.5 M sodium chloride solutions. Used sodium chloride was analytical grade.

The electrochemical corrosion tests (Electrochemical impedance spectroscopy—EIS and potentiodynamic polarization—PP) were performed in the conventional three-electrode cell system with a calomel reference electrode (SCE) and a platinum auxiliary electrode (Pt) using BioLogic corrosion measuring system with PGZ 100 measuring unit. The time for potential stabilization between the specimen and the electrolyte was set to 10 min. The exposed area of a specimen was 1 cm^2. An overview of the specimen designations for the PP and EIS tests is given in the Table 1.

Table 1. Overview of the specimen designations.

Specimen designation	Type of surface / solution
AR 0.05	As received, non-treated/ 0.05 M NaCl
AR 0.5	As received, non-treated/ 0.5 M NaCl
PN 0.05	Plasma nitrided/ 0.05 M NaCl
PN 0.5	Plasma nitrided/ 0.5 M NaCl

Electrochemical impedance spectroscopy measurements were recorded at the corrosion potential over a frequency range from 100 KHz to 5 mHz (10 points per decade, 10 mV R.M.S amplitude). Results of were displayed as the Nyquist plots. The representative Nyquist curve was selected from three measurements for the same type of surface conditions (AR/PN and the same composition of solution (0.05 M/0.5 M). The EIS parameter values were obtained by EC-LAB software analysis of the Nyquist curves.

The potentiodynamic polarization curves were recorded at the sweep rate of 1 mV/s, a potential scan range was applied between -0.3 and 0.8 V vs. open circuit potential (OCP). At least three experiment repeats were carried out for each combination of conditions (AR/ PN surface; 0.05 M/0.5 M solution) and the representative curve was selected.

3. Results and Discussion

3.1. Characterization of the Nitrided Layer

As the result of the applied PN process the nitrided surface layer (approx. 45 μm thickness) observable by OM in the specimen cross-section was formed (Figure 1). The morphology of the nitrided surface obtained by SEM analysis is presented in Figure 2a. As can be seen, the resulting surface is discontinuous and rough and exhibits an uneven distribution of chromium and nitrogen (Figure 2b).

 doi:10.20944/preprints202407.0971.v1

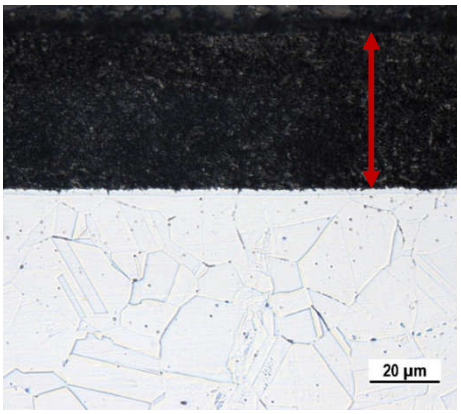

Figure 1. Cross-section edge of the plasma nitrided specimen: OM, Glycerine + nitric acid + hydrofluoric acid etch.

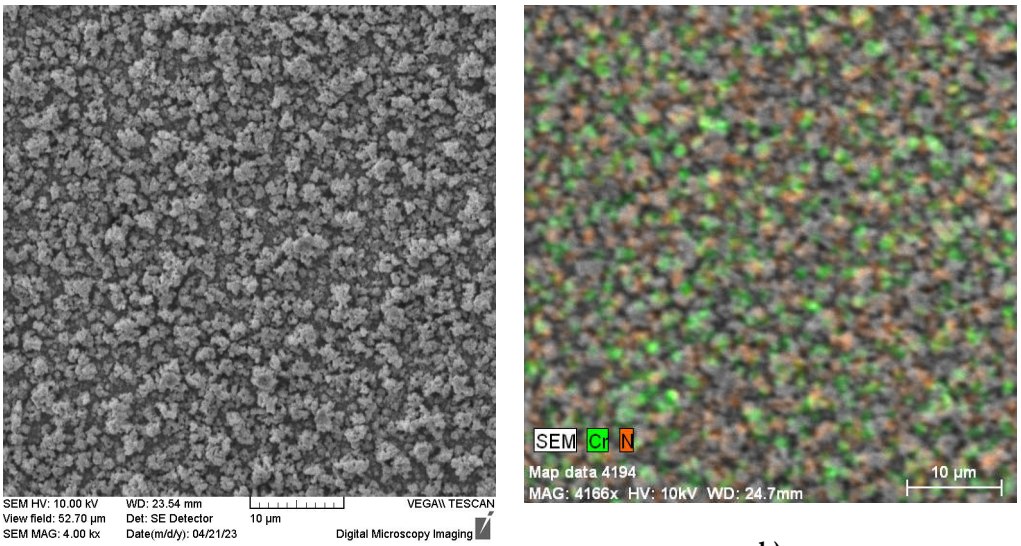

Figure 2. Plasma nitrided surface of AISI 304 specimen: a) morphology shown by SEM; b) distribution of chromium and nitrogen shown by EDX analysis.

The performed XPS analysis aimed to identify the chemical states of chromium (Figure 3a) and nitrogen (Figure 3b). If not indicated otherwise, the identification of their chemical states was carried out using the NIST X-ray Photoelectron Spectroscopy Database [30]. Chromium exists in two chemical states; before surface cleaning (the $Cr2p_{3/2}$ peak at a binding energy of 575.87 eV indicate presence of chromium in nitrogen environment [31], while the peak at an energy of 577.17 eV can be assigned to Cr_2O_3 [31,32] or chromium(III) hydroxide $Cr(OH)_3$ [32]. In addition, chromium satellite lines appeared at energies of 587.71 eV and 596.91 eV. After surface cleaning, slight shifts of main peaks were observed; the $Cr2p_{3/2}$ peak corresponding to Cr_2N appeared at a binding energy of 574.73 eV [33], and the peak corresponding to Cr_2O_3 at 576.77 eV [34]. The N1s line revealed nitrogen present in multiple chemical states, predominant contribution to the N1s line corresponds to chromium nitrides. N1s peak at 396.13 eV observed before surface cleaning can be identified as oxynitride, whereas for sputtered surface peak at 396.83 eV can be assigned to Cr_2N [35]. The Cr_2N phase was also confirmed by the authors [13,15] after high-temperature nitriding of austenitic stainless steels.

Preprints.org (www.preprints.org) | NOT PEER-REVIEWED | Posted: 12 July 2024 doi:10.20944/preprints202407.0971.v1

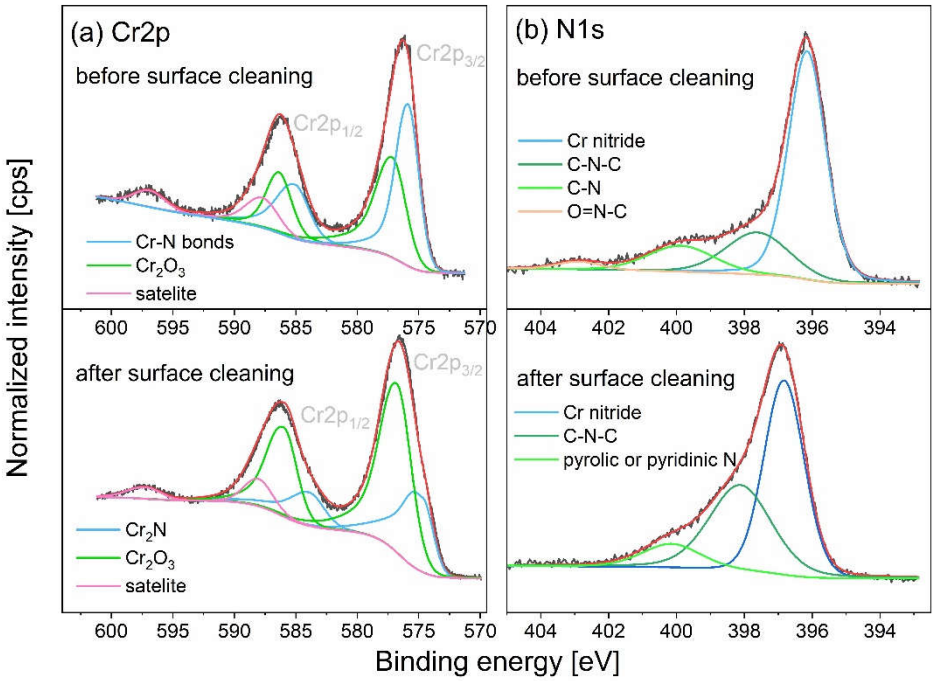

Figure 3. High resolution spectra of chromium and nitrogen: a) Cr2p, b) N1s.

The nitriding temperature used obviously ensured the sufficient solubility and the appropriate kinetic conditions for the intensive diffusion of nitrogen atoms into the surface layer of the material and their reactions with chromium. Due to the sufficient thermal energy of chromium atoms, the formation of chromium nitride was thermodynamically favored unlike the lower temperatures at which the driving force for the formation of stable nitride phases is insufficient [36,37].

3.2. Micro-Hardness Measurement

The sequence of micro-hardness measurement after PN and the obtained values are documented in Figure 4. The micro-hardness of the nitrided layer ranged from 1143 to 1572 HV 0.01, followed by a steep transition to of the softer part of the specimen with the micro-hardness values between 223 and 286 HV 0.01. The high hardness of the material after PN at the temperatures above 500°C is related to the Cr_2N chromium nitride, which was formed under these conditions (chapter 3.1) and significantly increased the hardness of the material [7,14,15,38,39]. A comparable values of the PN layer micro-hardness (about 1300 HV) on austenitic stainless steel plasma nitrided at 520 °C were recorded by de Araújo et. al. [15].

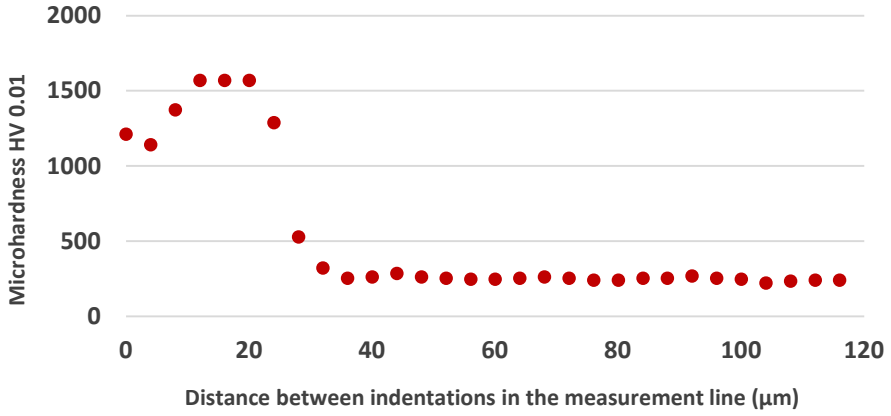

a)

Preprints.org (www.preprints.org) | NOT PEER-REVIEWED | Posted: 12 July 2024 doi:10.20944/preprints202407.0971.v1

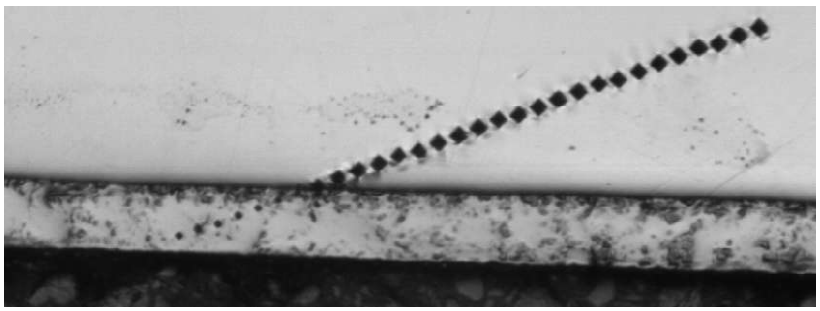

b)

Figure 4. Course of AISI 304 micro-hardness after plasma nitriding: a) graph of micro-hardness, b) measurement line.

3.2. Potentiodynamic Polarization (PP)

PP curves for the as received (non-treated) and plasma nitrided surfaces in both 0.05 M and 0.5 M NaCl solutions are shown in Figure 5 and Figure 6 respectively. The values of PP parameters are listed in Table 2. While the curves in Figure 5 are typical for passivating metals, the curves for plasma nitrided surfaces are without passive anodic branches and they express the state of the active corrosion (Figure 6). This essential difference in the curves shape points to the different control of anodic dissolution rate. The dissolution rate for passivating metals is controlled by passive current density, for actively corroding metal by corrosion current density. Therefore AR 0.05 and AR 0.5 curves were evaluated by the corrosion potential E_{corr} and the pitting potential E_p (Table 2). E_{corr} was identified directly from the curve as the potential of the transition from the cathodic to the anodic branch. E_p, denoting the breakdown of the passive film and the start of the stable pit growth, was determined as the potential of the strong continual increase of the current density in the passivity region. The PP parameters E_{corr}, i_{corr} (corrosion current density) and v_{corr} (corrosion rate), for PN 0.05 and PN 0.5 curves (Figure 6), were obtained as the result of the Tafel extrapolation using EC-LAB software.

Table 2. Values of the potentiodynamic polarization parameters.

Specimen designation	Corrosion Potential E_{corr} (V vs SCE)	Pitting potential E_p (V vs SCE)	Corrosion current density i_{corr} (10^{-3} mA/cm²)	Corrosion rate v_{corr} (mm/year)
AR 0.05	-0.16 ± 0.02	0.39 ± 0.04	-	-
AR 0.5	-0.18 ± 0.03	0.29 ± 0.05	-	-
PN 0.05	-0.30 ± 0.03	-	3.19 ± 0.19	0.04 ± 0.002
PN 0.5	-0.48 ± 0.05	-	6.81 ± 0.21	0.08 ± 0.002

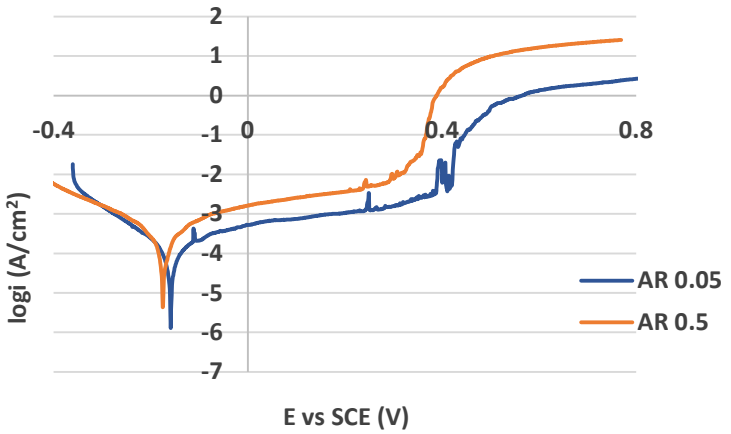

 doi:10.20944/preprints202407.0971.v1

Figure 5. Potentiodynamic polarization curves for as received AISI 304 in 0.05 M and 0.5 M sodium chloride solution.

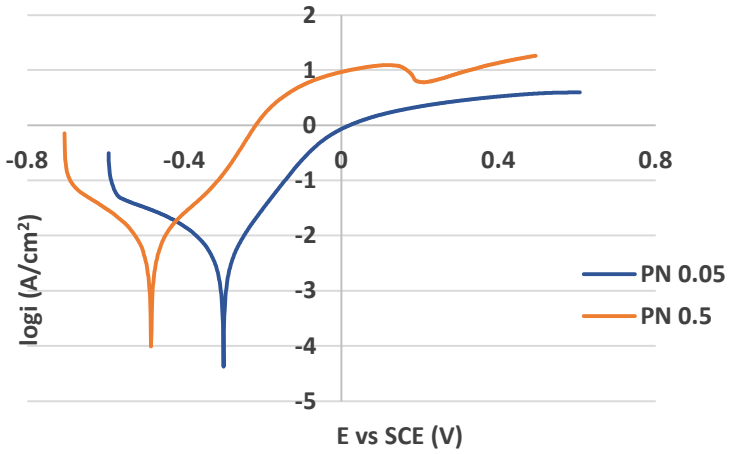

Figure 6. Potentiodynamic polarization curves for plasma nitrided AISI 304 in 0.05 M and 0.5 M sodium chloride solution.

According to the PP curves and the E_p values, the as received surfaces reflected adequate resistance to the pitting corrosion in both variously concentrated chloride solutions. Consistent with the published results [40–44] the higher chloride concentration induced the more intensive penetration of chloride anions through the weakened localities of the passive film and it led to a E_p drop compared to AR 0.05 E_p value (Table 2). The slight difference dependent on chloride concentration was also recorded in the thermodynamic stability expressed by E_{corr} values of AR 0.05 and AR 0.5 specimens.

As shown in Figure 6, the applied plasma nitriding process caused the passivity loss of PN specimens even at very low sodium chloride concentration (0.05 M solution). Kinetics of the corrosion process expressed by corrosion current density and corrosion rate point to an active corrosion in both solutions and decrease of E_{corr} values documents lower thermodynamic stability compared to the as received state (Table 2). Generally, the values of PP parameters (Table 2) indicate a reduced corrosion resistance in both solutions compared to the as received state. This result can be related to the precipitation of chromium nitride that depletes the surrounding areas of chromium, reducing the amount of the chromium atoms available to form the protective passive oxide film [15,16].

In addition, the presented rough morphology of the plasma nitrided surface (Figure 1a) with uneven distribution of nitrogen and chromium (Figure 1b) points to the presence of the discrete, separated chromium–nitrogen precipitates which do not form a continuous layer and enable the intensive scattered penetration of chloride anions into the material. The result is active corrosion during potentiodynamic polarization indicating a deterioration of the corrosion resistance of the plasma nitrided surface, which is not prevented even by low chloride concentration (0.05 mol/L).

De Araujo et al. [15] evaluated corrosion behavior of AISI 316L stainless steel after ionic plasma nitriding performed at 520 °C for 4 hours by potentiodynamic polarization in 0.6 M NaCl solution. In agreement with our results, they also recorded the loss of passivity and almost the same shape of the curve. The authors Kartikasari [16] came to the similar results for the same stainless steel plasma nitrided at 500 and 550 °C for 3 hours and tested by potentiodynamic polarization in unspecified chloride solution. Contrary to the findings above, Mareci et al. [45] recorded a strengthening of corrosion resistance in potentiodynamic polarization of plasma nitrided austenitic stainless steel (500 °C, 14 hours) in 0.5 M NaCl. The obtained results were attributed to a continuous smooth CrN layer prepared in glow discharge plasma nitriding unit [45].

3.3. Electrochemical Impedance Spectroscopy (EIS)

Preprints.org (www.preprints.org) | NOT PEER-REVIEWED | Posted: 12 July 2024 doi:10.20944/preprints202407.0971.v1

Similar to the authors [45–47] the evaluation of measured impedance spectra of the as received specimens was based on one time constant observed. Therefore a single loop circuit consisting of electrolyte resistance (R_Ω), charge transfer resistance (R_{ct}) and the constant phase element (CPE), was applied (Figure 7a). For the plasma nitrided specimens the two layer model of a porous surface film with two time constants containing R_Ω, R_{ct1}, R_{ct2}, CPE_1 and CPE_2 was used (Figure 7b), [45]. CPE represents the capacitor, if the "n" exponent present in the equation for the mathematical CPE expression equals one. The CPE values are affected by surface roughness, different thickness and coating's composition that are related to the kinetics of processes on the working electrode surface [48,49].

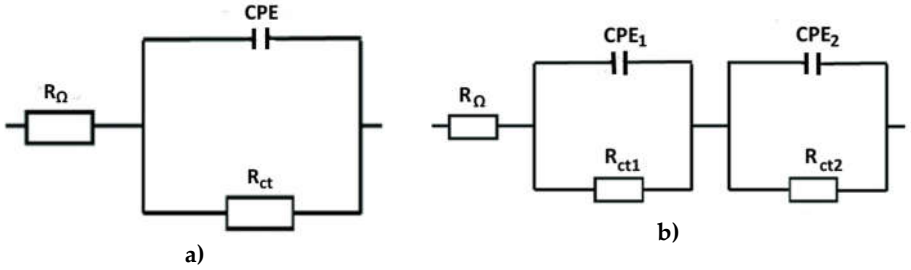

Figure 7. Equivalent circuits for the fitting of the impedance data: a) circuit with one time constant, b)circuit with two time constants.

The Nyquist plots obtained from EIS measurement are displayed in Figure 8 and Figure 9. The values of the fitted impedance parameters are presented in Table 3 and Table 4. The values of charge transfer resistances R_{ct} for the as received surfaces, derived from the Nyquist curves (Figure 8) confirmed the presence of the passive surface film recorded also at the PP measurement [50]. In contrast to the PP measurement, the effect of the chloride concentration on the quality and resistance of the passive oxide film was more pronounced during the EIS measurement (almost 6x lower R_{ct} in 0.5 M NaCl solution compared to 0.05 M solution). A significant decrease in the R_{ct} of AISI 304 stainless steel with a rise in the concentration of NaCl solution was also noted by Yin [44].

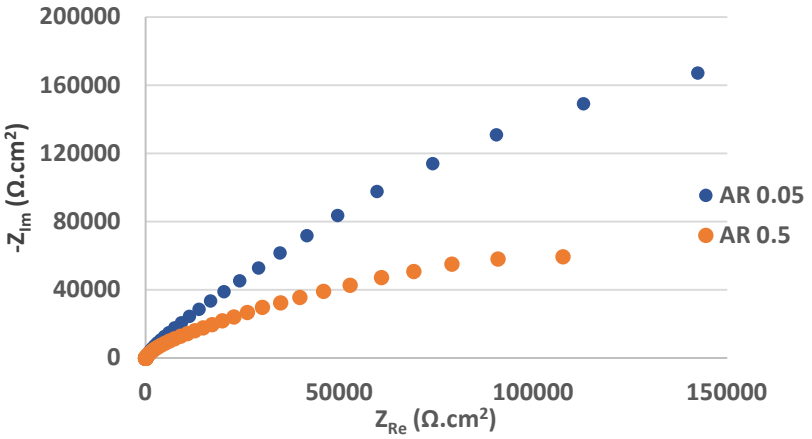

Figure 8. Nyquist curves for as received AISI 304 in 0.05 M and 0.5 M sodium chloride solution.

Preprints.org (www.preprints.org) | NOT PEER-REVIEWED | Posted: 12 July 2024 doi:10.20944/preprints202407.0971.v1

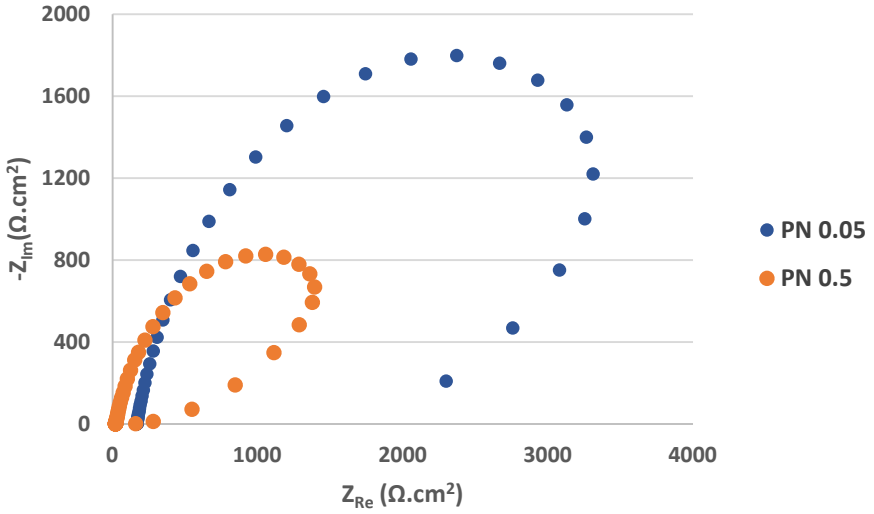

Figure 9. Nyquist curves for plasma nitrided AISI 304 in 0.05 M and 0.5 M sodium chloride solution.

Table 3. Values of the fitted impedance parameters for as received specimens: R_Ω—electrolyte resistance, R_{ct}–charge transfer resistance, CPE—constant phase element, n—exponent.

Specimen designation	R_Ω (kΩ.cm²)	R_{ct} (kΩ.cm²)	n	CPE (μF/cm²)
AR 0.05	0.161 ± 0.004	236.68 ± 0.9	0.85 ± 0.003	24.64 ± 0.12
AR 0.5	0.019 ± 0.002	40.68 ± 0.2	0.85 ± 0.002	33,5 ± 0.18

Table 4. Values of the fitted impedance parameters for plasma nitrided specimens: R_Ω—electrolyte resistance, R_{ct1}, R_{ct2}—charge transfer resistances, CPE_1, CPE_2—constant phase elements, n_1, n_2—exponents.

Specimen designation	R_Ω (kΩ.cm²)	R_{ct1} (kΩ.cm²)	R_{ct2} (kΩ.cm²)	CPE_1 (μF/cm²)	CPE_2 (μF/cm²)	n_1	n_2
PN 0.05	0.122 ± 0.003	2,11 ± 0.1	3.37 ± 0.2	247 ± 1.2	14.82 ± 0.8	0,87 ± 0.002	0.50 ± 0.002
PN 0.5	0.018 ± 0.002	1.95 ± 0.1	1.76 ± 0.2	376 ± 1.4	6.11 ± 0.2	0.82 ± 0.002	0.75 ± 0.002

According to the EIS results (Figure 9, Table 4), the total R_{ct} values (R_{ct1} + R_{ct2}) i.e., 4.48 kΩ.cm² for PN 0.05 and 3.71 kΩ.cm² for PN 0.5 specimens are very low and less dependent on chloride concentration compared to AR ones. It points to the increased electrical conductivity of the plasma nitrided surface leading to an acceleration of ongoing electrochemical reactions [49].

A higher electrical conductivity can be related to the discontinuous plasma nitride surface (Figure 1a) with more active sites for an adsorption and penetration of chloride anions and consequently for efficient charge transfer processes. Moreover, the precipitation of chromium nitrides causes chromium depletion in adjacent areas, supports suppression of passive oxide film and facilitates easier electron transfer [13,16,36].

4. Conclusions

 doi:10.20944/preprints202407.0971.v1

- Plasma nitriding of AISI 304 stainless steel performed at the temperature of 530 °C for 24 hours induced the formation of a nitrided surface layer (thickness approx. 45 μm) with rough discontinuous surface and with an uneven distribution of nitrogen and chromium.
- XPS analysis of the surface nitride layer proved the presence of bonds between chromium and nitrogen. Predominant contribution to the N1s line corresponds to chromium nitrides, sputtered surface peak at 396.83 eV can be assigned to Cr_2N phase. This phase was also confirmed by the Cr2p3/2 peak appeared at a binding energy of 574.73 eV.
- The plasma nitriding process significantly increased the micro-hardness of the surface layer compared to the inner parts of the material (1143 to 1572 HV 0.01 in the nitride layer, 223 to 286 HV 0.01 in the inner part).
- Potentiodynamic polarization revealed the loss of the passive behavior of the material after plasma nitriding in both solutions—the shape of PP curves and the i_{corr} values obtained by Tafel analysis (Table 2) are typical for an actively corroding metal.
- The results of EIS measurements show a significant decrease in total R_{ct} values after plasma nitriding (Table 3, Table 4), which means an increase in the rate of electrochemical reactions at the material/solution interface.

It can be stated, that the results of EIS and potentiodynamic polarization measurements are in good agreement and they confirmed a significant reduction in corrosion resistance after plasma nitriding (530 °C/24 hours), even in a solution with a very low concentration of chlorides (0.05 mol/L). Therefore, it is not recommended to use AISI 304 steel thermo-chemically treated in the above-described way in any chloride solutions.

Author Contributions: Conceptualization, V.Z.; methodology, V.Z., K.B., M.S.; software, M.S., K.B.; validation, V.Z., P.D., L.M; investigation, V.Z., K.B.; resources, M.S., L.M., P.D.; writing—original draft preparation, V.Z.; writing—review and editing, V.Z.; visualization, K.B., P.D.; supervision, V.Z; project administration, L.M.

Funding: The research was funded by Scientific Grant Agency of Ministry of Education, Science and Sport of Slovak Republic and Slovak Academy of Sciences grant KEGA 016ŽU-4/2023.

Institutional Review Board Statement: Not applicable.

Informed Consent Statement: Not applicable.

Data Availability Statement: Data sharing is not applicable to this article.

Conflicts of Interest: The authors declare no conflict of interest.

References

1. Saravanan, M.; Deveraju, A.; Venkateshwaran, N.; Krishnakumari, A.; Saarvesh, J. A review on recent progress in coatings on AISI austenitic stainless steel. *Mater. Today Proc.* **2018**, part 2, 5, 6, 14392-14396.
2. Lai, J.K.L.; Lo, K.H.; Shek, C.H. Austenitic stainless steel. In. *Stainless steels: An introduction and recent developments*. Bentham Science Publexecutive STE Y-2, Sharjah, U Arab Emirates, 2012; pp. 23-40.
3. Lipińsky T. Investigation of corrosion rate of X55CrMo14 stainless steel at 65% nitrate acid at 348 K. *Prod. Eng. Arch.* **2021**, 27, 2.
4. Chvalníková, V.; Uhríčik, M.; Palček, P.; Slezák, M.; Šikyňa, L.; Drímalová, P. Austenitic steel AISI 304 under static and cyclic loading. *Manuf. Technol.* **2023**, 23, 5, 623-629.
5. Kovács, D.; Dobránszky, J. Effects of Thermochemical Surface Treatments on the Industrially Important Properties of X2CrNiMo 17-12-2 Austenitic Stainless Steel. *Period. Polytech. Mech. Eng.* **2019**, 63, 3, 214-219.
6. Zhang, Z.; Bi, Y. ; Zhang, M.; Li, Y.; Zhao, F.; Zhang, S.; He, Y. Properties of stainless-steel surface after hollow cathode assisted plasma nitriding. *Mater. Res. Express* **2020**, 7, 116524.
7. Wang, L. Surface modification of AISI 304 austenitic stainless steel by plasma nitriding. *Appl. Surf. Sci.* **2003**, 211, 308–314.
8. Baranowska, J.; Arnold, B. Corrosion resistance of nitrided layers on austenitic steel. *Surf. Coat. Technol.* **2006**, 200, 6623–6628.

9. Zhou, Y.L.; Xia, F.; Xie, A.J.; Peng, H.P.; Wang, J.H.; Li, Z.W. A Review—Effect of Accelerating Methods on Gas Nitriding: Accelerating Mechanism, Nitriding Behavior, and Techno-Economic Analysis. *Coatings* **2023**, 13, 11, 1846.
10. Funch, C.V.; Christiansen, T.L.; Somers, M.A.J. Gaseous nitriding of additively manufactured maraging steel; nitriding kinetics and microstructure evolution. *Surf. Coat. Technol.* **2022**, 432, 128055.
11. Escalada, L.; Dalibon, E.L.; Brühl, S.P.; Manova, D.; Mändl, S.; Simison, S. Influence of Inclusions in the Corrosion Behavior of Plasma Nitrided Stainless Steel. *Adv. Eng. Mater.* **2023**, 2201112.
12. Biehler, J.; Hoche, H.; Oechsner, M.; Kaestner, P.; Bunk, K.; Bräuer, G. Influence of the microstructure on the corrosion resistance of plasma-nitrided austenitic stainless steel 304L and 316L. *Materialwiss. Werkstofftech.* **2014**, 45, 10.
13. Olzon-Dionysio, M.; Olzon-Dionysio, D.; Campos, M.; Takemitsu Shigeyosi, W.; De Souza, S.D.; De Souza, S. Corrosion resistance of AISI 316L plasma nitrided at different temperatures and times. *Hyperfine Interact.* **2019**, 240, 26.
14. Lanzoni, F; Cislaghi, L.; Sisti, V.; Trasatti, S. Influence of process parameters of plasma nitriding on corrosion resistance of stainless steels. *Metall. Ital.* **2014**, 2, 27-33.
15. De Araújo, E.; Marinho Bandeira, R.; Dorigão Manfrinato, M.; Aparecido Moreto, J.; Borges, R.; Santos Valese, S.; Atsushi Suzuki, P.; Sgarbi Rossino, L. Effect of ionic plasma nitriding process on the corrosion and micro-abrasive wear behavior of AISI 316L austenitic and AISI 470 super-ferritic stainless steels. *JMR&T* **2019**, 8, 2, 2180-2191.
16. Kartikasari, R.; Sutrisna, A.; Aziz, I. Corrosion Behavior of Plasma Nitrided SS316L Biomaterial. *Open Mater. Sci.* **2017**, 11, 29-37.
17. Flis-Kabulska, I.; Sunb, Y.; Flis, J. Monitoring the near-surface pH to probe the role of nitrogen in corrosion behaviour of low-temperature plasma nitrided 316L stainless steel. *Electrochim. Acta* **2013**, 104, 208–215.
18. Mukherjee, S.; Raole, P.M.; Kumar, A.; Chattoraj, I.; Rao, K.R.M.; Manna, I. Studies on low-energy nitrogen plasma immersion ion implantation on austenitic stainless steel and Cu-strengthened HSLA-100 steel. *Surf. Coat. Technol.* **2004**, 186, 282-286.
19. Gupta, D. Plasma Immersion Ion Implantation (PIII) Process-Physics AND Technology. *Int. J. Adv. Technol.* **2011**, 2, 471–490.
20. Liu, C.L.; Chu, P.K.; Lin, G.Q.; Qi, M.: Anti-corrosion characteristics of nitride-coated AISI 316L stainless steel coronary stents. *Surf. Coat. Technol.* **2006**, 201, 2802–2805.
21. Adachi, S.; Egawa, M.; Yamaguchi, T.; Ueda, N. Low-Temperature Plasma Nitriding for Austenitic Stainless Steel Layers with Various Nickel Contents Fabricated via Direct Laser Metal Deposition. *Coatings* **2020**, 10, 4, 365.
22. Saravanan, P.; Raja, V.S.; Mukherjee, S. Effect of plasma immersion ion implantation of nitrogen on the wear and corrosion behavior of 316LVM stainless steel. *Surf. Coat. Technol.* **2007**, 201, 8131–8135.
23. Borgioli, F.; Galvanetto, E.; Bacci, E. Low temperature nitriding of AISI 300 and 200 series austenitic stainless steels. *Vacuum* **2016**, 127, 51–60.
24. Borgioli, F. The Corrosion Behavior in Different Environments of Austenitic Stainless Steels Subjected to Thermochemical Surface Treatments at Low Temperatures: An Overview. *Metals* **2023**, 13, 4, 776.
25. Mumtaz, K.; Takahashi, S.; Echigoya, J.; Zhang, L.; Kamada, Y.; Sato, M. Temperature dependence of martensitic transformation in austenitic stainless steel. *J. Mater. Sci.* **2003**, 22, 423—427.
26. Manova, D.; Eichentopf, I.M.; Hirsch, D.; Mändl, S.; Neumann, H.; Rauschenbach, B. Influence of Microstructure on Nitriding Properties of Stainless Steel. *IEEE Trans. Plasma Sci.* **2006**, 34, 4, 1136-1140.
27. Bhadeshia, H.; Honeycombe, R. Stainless steels*:* Microstructure and properties. In: *Steels*, Bhadeshia, H. and Honeycombe, R., Eds., Elsevier Ltd., Amsterdam, 2017; pp. 343-376.
28. Li, Y.; Wang, Z.; Wang, L. Surface properties of nitrided layer on AISI 316L austenitic stainless steel produced by high temperature plasma nitriding in short time. *Appl. Surf. Sci.*, **2014**, 298, 15, 243-250.
29. Li, Y.; He, Y.Y.; Zhang, S.Z.; Wang, W.; Zhu, Y.J. Microstructure and corrosion resistance of nitrogen-rich surface layers on AISI 304 stainless steel by rapid nitriding in a hollow cathode discharge. *Appl. Phys. A-Mater.* **2018**, 124, 1, 65.
30. NIST X-ray Photoelectron Spectroscopy Database, NIST Standard Reference Database Number 20, National Institute of Standards and Technology, Gaithersburg MD, 2000, 20899.
31. Lippitz, A.; Hübert, T. XPS investigations of chromium nitride thin films, *Surf. Coat. Technol.* **2005**, 200, 1–4, 250-253.
32. Moffat, T.P.; Latanision, R.M.; Ruf, R.R. An X-ray photoelectron spectroscopy study of chromium-metalloid alloys—III, *Electrochim. Acta* **1995**, 40, 11, 1723-1734.
33. Nishimura, O.; Yabe, K.; Iwaki, M. X-ray photoelectron spectroscopy studies of high-dose nitrogen ion implanted-chromium: a possibility of a standard material for chemical state analysis, *J. Electron Spectros. Relat. Phenomena* **1989**, 49, 3, 335-342.
34. Sleigh, C.; Pijpers, A.P.; Jaspers, A.; Coussens, B.; Meier, R.J. On the determination of atomic charge via ESCA including application to organometallics, *J. Electron Spectros. Relat. Phenomena* **1996**, 77, 1, 41-57.

35. Yuan, Y.; Zhang, B.; Sun, J.; Jonnard, P.; Le Guen, K.; Tu, Y.; Lan, R. Structure and optical properties of CrOxNy films with composition modulation. *Surf. Eng.* **2019**, 36, 4, 411–417.
36. Tenelanda-Osorio, L.I.; Vélez, M.E. First principles study of the thermodynamic, mechanical and electronic properties of crystalline phases of Chromium Nitrides. *J. Phys. Chem. Solids* **2021**, 148, 109692.
37. De Las Heras, E.; Ybarra, G.; Lamas, D.G.; Cabo, A., Dalibon, E.L.; Brühl, S.P. Plasma nitriding of 316L stainless steel in two different N_2-H_2 atmospheres - Influence on microstructure and corrosion resistance. *Surf. Coat. Technol.* **2017**, 313, 15, 47-54.
38. Yetim, A. F.; Yildiz, F.; Alsaran, A.; Celik, A. Surface modification of 316L stainless steel with plasma nitriding. *Kovove Mater.* **2008**, 46, 2, 105-116.
39. Scheuer, C.J.; Zanetti, F.I.; Cardoso, R.P.; Brunatto, S.F. Influence of process temperature on phase formation in plasma nitride AISI 420 steel. In Proceedings of the 22º CBECiMat - Congresso Brasileiro de Engenharia e Ciência dos Materiais 06 a 10 de Novembro de 2016, Natal, RN, Brasil.
40. Saefuloh, I.; Kanani, N.; Gumelar Ramadhan, F.; Rukmayadi, Y.; Yusuf, Y.; Abdullah, S.; Susilo, S. The Study of Corrosion Behavior and Hardness of AISI Stainless Steel 304 in Concentration of Chloride Acid Solution and Temperature Variations. *J. Phys. Conf.* **2020**, 1477, 052058.
41. Liu, W.; Yang, H.; Li, X.; Zhang, Z.; Lin, Y.; Deng, K. Effect of Chloride and Iodide on the Corrosion Behavior of 13Cr Stainless Steel. *Metals* **2022**, 12, 11, 1833.
42. Rustandi, A.; Setiawan, S.; Fathurrahman, I. The Effect of Sodium Chloride Concentration on Corrosion Resistance of Austenitic Stainless Steel 316L and SMA Weldment. *Sol. St. Phen.* **2017**, 263, 120-124.
43. Asaduzzaman, M.D.; Mustafa, C.M.; Islam, M. Effects of concentration of sodium chloride solution on the pitting corrosion behavior of AISI-304L austenitic stainless steel. *Chem. Ind. Chem. Eng. Q.* **2011**, 17, 4, 477–483.
44. Yin, Z. Effect of Chloride Ion Concentration on the Corrosion Behavior of 304 Stainless Steel Used in the Electric Water Heater. *Int. J. Electrochem. Sci.*, **2022**, 17, 220415.
45. Mareci, D.; Strugaru, S.I.; Munteanu, C.; Bolat G. Evaluation of the corrosion resistance of plasma nitrided austenitic stainless steel. *Int. J. Mater. Res. (formerly Z. Metallkd.)* **2015**, 106, 3, 267-274.
46. Brytan, Z.; Niagaj, R.; Reiman, L. Corrosion studies using potentiodynamic and EIS electrochemical techniques of welded lean duplex stainless steels UNSS82441. *Appl. Surf. Sci.* **2016**, 388, 160–168.
47. Noah, G. G.; Muruve, N. G.; Cheng, Y. F.; Feng, Y.; Liu, T.; Muruve, D. A.; Hasset, D. J.; Irvin, R. T. Peptide-based biocoatings for corrosion protection of stainless steel biomaterial in a chloride solution. *Mat. Sci. Eng.: C* **2016**, 68, 695-700.
48. Yuan, X. Z. R.; Song, C.; Wang, H.; Zhang, J. *Electrochemical impedance spectroscopy in PEM fuel cells: fundamentals and applications*; Springer – Verlag: London, 2010; pp. 39-93.
49. Hernández H. H.; Ruiz Reinoso A.M.; Trinidad Gonzáles, J.C.; González Morán, C.O.; Miranda Hernández, J. G. Electrochemical Impedance Spectroscopy (EIS): A Review Study of Basic Aspects of the Corrosion Mechanism Applied to Steels. Open Access peer-reviewed chapter 2020. Available online: https://www.intechopen.com/chapters/74147 (accessed on 17. June 2024).
50. Olsson, C.O.A.; Landolt, D. Passive films on stainless steels – chemistry, structure and growth, *Electrochim. Acta* **2003**, 48, 1093–1104.